

All-Dielectric Chiral Metasurfaces Based on Crossed-Bowtie Nanoantennas

Faustino Reyes Gómez,[†] J. Ricardo Mejía-Salazar,^{*,‡} and Pablo Albella^{*,§}

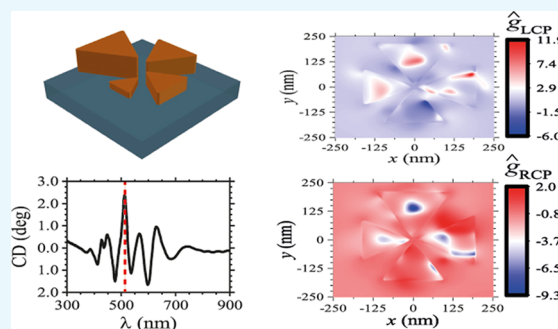
[†]Departamento de Física, Universidad del Valle, Cali AA 25360, Colombia

[‡]National Institute of Telecommunications (Inatel), Santa Rita do Sapucaí, MG 37540-000, Brazil

[§]Department of Applied Physics, University of Cantabria, Avda. Los Castros, s/n, Santander 39005, Spain

Supporting Information

ABSTRACT: Circular dichroism spectroscopy is a technique used to discriminate molecular chirality, which is essential in fields like biology, chemistry, or pharmacology where different chiral agents often show different biological activities. Nevertheless, due to the inherently weak molecular-chiroptical activity, this technique is limited to high concentrations or large analyte volumes. Finding novel ways to enhance the circular dichroism would boost the performance of these techniques. So far, the enhancement of light–matter interaction mediated by plasmons is the most common way to develop chiral plasmonic structures with extraordinarily strong chiroptical responses. However, absorptive losses of metals at optical frequencies has hindered its practical use in many scenarios. In this work, we propose an all-dielectric low-loss chiral metasurface with unit cells built by high-refractive-index crossed-bowtie nanoantennas. These unit cells, built of silicon, strongly increase the chiroptical effect through the simultaneous interaction of their electric and magnetic modes, which in contrast to other recent proposals shows at the same time a high concentration of the electric field in its gap that leads to the presence of hotspots. The proposed structure exhibits a circular dichroism spectra up to 3-fold higher than that of previous proposals that use complex plasmonic or hybrid nanostructures, making it a clear alternative to develop low-loss metasurfaces with potential applications in chiral target sensing/biosensing. For completeness, single triangular shaped and symmetric (achiral) bowtie nanostructures were also studied as possible candidates for a detection up to the single-molecule level due the lack of a circular dichroism background of the nanostructures themselves.



INTRODUCTION

Chirality refers to a geometrical or structural handedness of an object, meaning that its mirror image cannot be superimposed on itself. This phenomenon is ubiquitous in nature and plays a key role in life sciences, analytical chemistry, biochemistry, and medical sciences.^{1,2} An example of chiral structures in chemistry are the enantiomers, also known as optical isomers. In pharmacology, for example, different enantiomers have the same chemical structure, but their biological activities can make a significant difference between an effective treatment or an ineffective one (with serious side-effects).^{3,4} From the optical point of view, chiral materials present different refractive indexes when interacting with left circularly polarized (LCP) light or right circularly polarized (RCP) light, giving rise to optical activity (OA) and circular dichroism (CD).^{5,6} The first phenomenon consists of the rotation induced in the polarization plane of linearly polarized light (which is just a superposition of LCP and RCP lights) and the second is the difference in absorption when excited by left and right circularly polarized lights. Both phenomena are extremely connected by the Kramers–Kronig relations.

CD spectroscopy, that is, the differential absorption of left- and right-hand circularly polarized (LCP and RCP) light, is

traditionally used to discriminate molecular chirality.⁷ Nevertheless, due to the inherently weak molecular-chiroptical activity, this technique is limited to high concentrations or large analyte volumes. On the other hand, recent advances in metamaterials,^{8,9} optoelectronics,^{10–12} biosensing,^{13–15} enantioselective forces,^{16–18} nanometrology,¹⁹ and ultrafast data processing^{20,21} stem from the combined advances in the tailoring, patterning, and manipulation of light through confinement and enhancement at nanometric scales. The ability of plasmonic structures to localize and enhance light at dimensions much smaller than the incident wavelength,²² through the resonant coupling of electromagnetic waves to collective oscillations of free electrons in metals, has been extensively used for these purposes. In particular, the last few years have witnessed an explosive development of chiral plasmonic structures with extraordinarily strong chiroptical responses.^{23–35} However, absorptive losses associated with the inter- and intraband transitions in metals at optical frequencies constitute a major hurdle for practical use in many scenarios.

Received: July 29, 2019

Accepted: November 8, 2019

Published: December 2, 2019

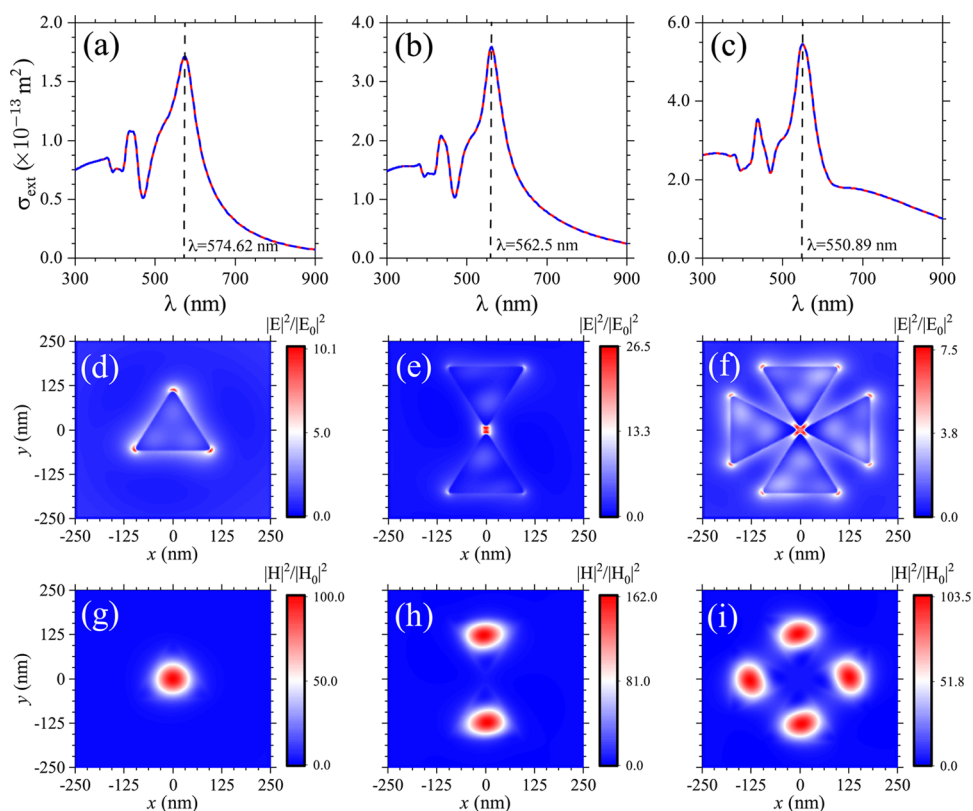


Figure 1. Extinction spectra, σ_{ext} for (a) a single triangular scatterer, (b) a dielectric bowtie nanoantenna, and (c) two crossed-bowtie nanoantennas. Triangular scatterers are considered as made of Si, with sides $l = 190$ nm and height $h = 100$ nm. The tip-to-tip gap was taken as $g = 20$ nm. Results for right/left circularly polarized (RCP/LCP) light, incident along the z -axis, are presented by solid/dashed (red/blue) lines. The corresponding electric and magnetic near-field intensities, at the highest resonance wavelengths, are presented in (d)–(f) and (g)–(i), respectively.

The use of high-refractive-index (HRI) dielectric nanostructures, where Ohmic losses inherent to metals can be significantly diminished, has emerged as a promising solution to control the near- and far-field optical response at the nanoscale.^{36,37} In contrast to their plasmonic counterpart, where the electromagnetic enhancement is governed only by electric resonances, HRI dielectric nanoparticles can exhibit both electric and magnetic resonances.^{38–40} Important applications are envisaged, like optical cloaking,⁴¹ harmonic generation,^{42,43} nanoscale lasers,⁴⁴ or directionality of light.^{45–48} Despite these advances, their use in some applications are limited by the relatively mild intensity of the electric-field enhancement and the occurrence of the magnetic hotspot inside the nanoparticles, thus being hard to access. To surpass these limitations, some recent works^{49,50} demonstrated that in analogy to plasmonic aggregates, ensembles of two or more dielectric particles exhibit large enhancements of the electric and magnetic fields in the gap (hotspots). Inspired by these works, here we propose an all-dielectric low-loss chiral metasurface with unit cells built by high-refractive-index crossed-bowtie nanoantennas. These unit cells, built of silicon, strongly increase the chiroptical effect through the simultaneous interaction of their electric and magnetic modes. Recent proposals⁵¹ use dielectric nanospheres of different sizes to produce CD signals, where the excitation of strong hotspots can be hindered by the curvilinear surface of the spheres. Our platform shows a high concentration of the electric field in its gap that leads to the presence of hotspots being directly accessible to nearby emitters, thus opening the route for new low-loss surface-enhanced spectroscopies, sensing, and other

applications in the field of nanophotonics. An additional advantage of the crossed-bowtie unit cell is that it can be excited at normal incidence, whereas in the case of spherical oligomers of different unit sizes, the electric field needs to be obliquely placed along the line joining two diameters to generate a hotspot. As a result, the proposed structure exhibits a circular dichroism spectra up to 3-fold higher than those of previous proposals that use complex plasmonic or hybrid nanostructures,⁵² making it a clear alternative to develop low-loss metasurfaces with potential applications in chiral target sensing/biosensing. We also highlight that this chiral structure can be spectrally tuned to exhibit its maximum circular dichroism at the desired wavelength by just engineering its size, shape, and periodicity.

RESULTS AND DISCUSSION

It is known that high-refractive-index dielectric nanoparticles, when excited with light, can retain the electromagnetic field inside due to the generation of strong displacement currents. This effect, for resonant frequencies, can lead to electric and/or magnetic resonant modes produced by the inner field distributions. Analogous to metallic nanoparticles, under surface plasmon resonance conditions, HRI dielectric particles can also exhibit enhanced electric field distributions at their boundaries. When resonant nanoparticles, metallic or dielectric, are coupled, forming dimers, trimers, or more complex aggregates, their electric modes in the case of plasmonics, and electric and magnetic modes in the case of dielectrics, overlap and lead to an enhancement and spectral shift of the extinction cross sections. Figures 1a–c show the extinction spectra of a

single triangular scatterer, a bowtie, and two crossed bowtie scatterers, respectively. All of them made of amorphous silicon⁵³ and surrounded by air. They are illuminated by left and right circularly polarized plane waves with the wavevector perpendicular to them and along the z -axis. These systems were considered as deposited on a glass ($n_g = 1.5$) substrate and surrounded by air. The corresponding extinction spectra, $\sigma_{\text{ext}} = \sigma_{\text{scat}} + \sigma_{\text{abs}}$, were numerically calculated with the finite-difference time-domain (FDTD) method. σ_{scat} and σ_{abs} correspond to the scattering and absorption cross sections associated with each platform. The length of the side and the height of each triangle is constant here, $l = 190$ nm and $h = 100$ nm, to keep their resonances in the optical range and a tip-to-tip length of 20 nm. The optical constants for silicon were obtained from Palik.⁵³

Three overlapping peaks with a small difference in width, amplitude, and spectral position can be clearly identified in all cases for incident wavelengths of $\lambda \approx 570$, 520, and 430 nm, corresponding to magnetic dipolar, electric dipolar, and magnetic quadrupolar resonances, respectively.⁴⁹ We observe that both the magnetic and the electric resonances are slightly shifted (the magnetic resonance to the blue and the electric resonance to the red), and their intensities vary consequently. In the same way that metallic nanoparticles can concentrate electric fields in small volumes, when dielectric nanoparticles are coupled to form dielectric antennas, they also provide a reasonably strong electric field enhancement and localization of electromagnetic energy in the antenna gap. Calculations demonstrate that intense and localized electric and magnetic near-fields are present in the gap of dielectric bowties and crossed-bowties. Figures 1d–f,g–i show that the normalized electric and magnetic near-fields for LCP incident light at the magnetic resonance wavelength exhibit a rotational symmetry on the xy plane in all cases, leading to a lack of optical chirality, that is, $\sigma_{\text{RCP}} = \sigma_{\text{LCP}}$. This can also be understood in terms of the mirror symmetry along the z -axis that all of the systems present. However, we must remark here that all of these nonchiral structures have an associated near-field optical chirality, C , at each resonance, as can be observed in Figure S1 of the Supporting Information. The optical chirality, $C = -\frac{\epsilon_0 \omega}{2} \text{Im}(\mathbf{E}^* \cdot \mathbf{B})$, quantifies the interaction strength of the electromagnetic field with the chiral photonic structure, thus being responsible for the CD spectroscopic signal. This term reaches its maximum value, $C_{\text{CPL}}^{\pm} = \pm \frac{\omega \epsilon_0}{2c} |\mathbf{E}|^2$, for circularly polarized light (CPL) in free-space.⁵⁴ Hence, the enhancement of the electric and magnetic field amplitudes, for which $\text{Im}(\mathbf{E}^* \cdot \mathbf{B}) \neq 0$, is a key element to improve the CD signal.⁵⁴

The first approach to introduce chiral optical activity in the system consists of breaking the mirror symmetry of the structure along the z -axis. This can be done in three different ways: changing the side lengths of each arm, the heights, and both together, as depicted in Figures 2a–c, respectively. The corresponding CD signal for each case, in the extinction spectra, is calculated as follows²⁹

$$\text{CD} = \tan^{-1} \left(\frac{\sigma_{\text{RCP}} - \sigma_{\text{LCP}}}{\sigma_{\text{RCP}} + \sigma_{\text{LCP}}} \right) \quad (1)$$

with σ being the extinction cross section for RCP and LCP illumination, which was calculated via the commercial software

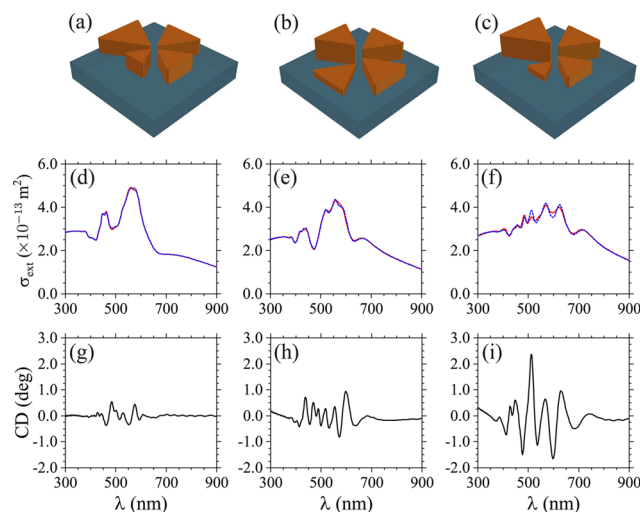


Figure 2. Crossed-bowtie nanoantennas with a broken mirror symmetry along the z -axis by changing the (a) side lengths, (b) heights, and (c) simultaneously the heights and side lengths of the building dielectric scatterers. (d–f) Extinction spectra, σ_{ext} , of the systems shown in (a)–(c), respectively, for RCP/LCP incident light are presented by solid/dashed (red/blue) lines. Results were calculated for systems with symmetry breaking by changing the (a) side lengths, (b) heights, and (c) side lengths and heights, simultaneously, for the building dielectric scatterers. (g–i) CD spectra calculated for the systems (a)–(c), respectively.

Lumerical FDTD, for wavelengths in the range from $\lambda = 300$ to 900 nm, and considering all of the media as isotropic.

In the first case, shown in Figure 2a, side-lengths of the dielectric triangles were increased from 170 to 230 nm, in steps of 20 nm, following the anticlockwise direction. A small differences in the extinction spectra of the system is observed (Figure 2d), thus producing a negligible effect in the CD spectral response, as can be seen in Figure 2g. A second symmetry-breaking procedure consisted of varying the scatterer heights from 80 to 140 nm, in steps of 20 nm, following the anticlockwise sense, as depicted in Figure 2b. Although differences in the extinction spectra remain small (see Figure 2e), the CD amplitude was slightly increased when compared with the previous case, as noted from Figures 2g and 2h. In the last case, we simultaneously changed the side lengths and heights, in steps of 20 nm, again following the anticlockwise direction. The latter case is depicted in Figure 2c. The corresponding extinction spectra, for RCP and LCP incident lights, are plotted in Figure 2f. In this case, we find the largest CD signal, as noted from Figure 2i, showing this configuration as a clear candidate to be used later as the periodic unit cell for the design of a two-dimensional chiral all-dielectric metasurface. We must remark that the studied chiral platforms present enhanced and robust CD signals, in contrast to previous plasmonic proposals⁵² requiring precise control of the cooling and the seed structure to exhibit an about three times smaller chiroptical activity.

As mentioned before, enhanced CD signals require the enhancement of the electric and magnetic near-fields to produce higher $\text{Im}(\mathbf{E}^* \cdot \mathbf{B})$ terms. A deep insight can be obtained from the electric and magnetic field maps in Figure 3. The near-field maps are only shown for the wavelengths corresponding to the maximum amplitudes of the CD signal extracted from Figures 2h,i. Thus, Figures 3a,b [e,f] and Figures 3c,d [g,h] are for RCP [LCP] polarization at

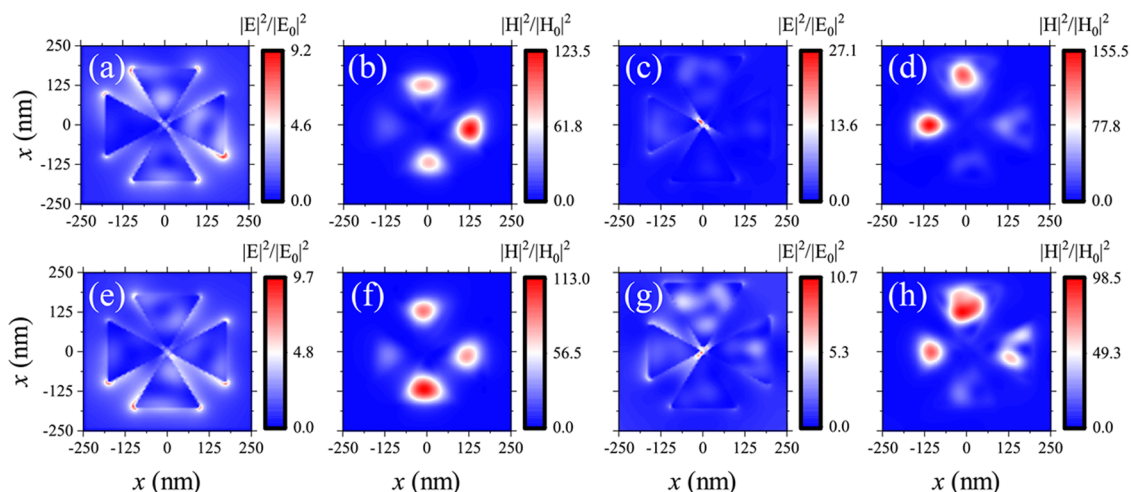


Figure 3. Near-field profiles for RCP and LCP incident lights, (a–d) corresponding to the wavelength ($\lambda = 597.122$ nm) of the maximum amplitude in Figure 2h and (e)–(h) to the wavelength ($\lambda = 511.294$ nm) of the maximum amplitude in Figure 2i, are presented in the upper and lower panels, respectively.

$\lambda = 597.12$ and 511.29 nm, respectively. In the case of Figures 3a,b and Figures 3e,f, we can observe that there is only a small difference for the interaction of RCP and LCP incident lights with the structure, where the electric hotspots are mainly located at the external boundaries of the scatterers and the magnetic fields only exhibit a small difference in their amplitudes. On the other hand, Figures 3c,d and Figures 3g,h exhibit strong changes in their amplitudes and symmetries, with the additional advantage of having the hotspots located at the gap region. The latter hotspots can be exploited to improve light–molecule interactions in chiral-sensing applications, for example, by placing a chiral molecule at the gap region. The optical chiralities for these structures, associated with each resonance, are shown in Figure S2 of the Supporting Information.

To show the robustness of our proposal, the effects induced by small shifts and asymmetries, in the tip-to-tip gaps of the system described in Figure 2c, were also studied. In Figures 4a,b, we considered two different possibilities, as illustrated in the corresponding insets. In the first case, we considered a small misalignment of 10 nm around the center of both

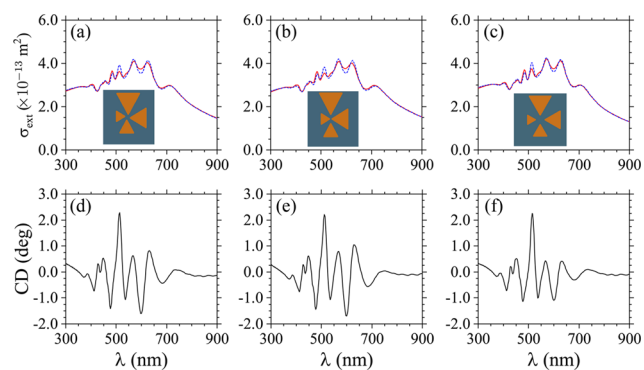


Figure 4. RCP (solid) and LCP (dashed) scattering spectra for the system in Figure 2f under misalignment and asymmetries. A misalignment of 10 nm around the center was considered in (a) (see inset). In (b), different tip-to-tip gap sizes, 20 and 30 nm, were used (see inset). Symmetric gaps of 40 nm were considered in (c) (see inset). The corresponding CD spectra are presented in (d)–(f).

crossed bowties (see Figure 4a). In the second, we explored two different tip-to-tip gap distances, 20 and 30 nm, for the longitudinal and transversal bowties, respectively, as depicted in Figure 4b. The extinction spectra, for RCP and LCP polarizations, do not suffer any considerable change when compared with the ones in Figure 2c, thus indicating a robust behavior. The same can be concluded for the corresponding CD spectra in Figures 4d,e when compared with results in Figure 2i. Another feature we explored was to double the gap sizes in Figure 2f (20 nm), that is, using gaps of 40 nm. The latter results are presented in Figures 4c,f, from where a small decrease in the CD amplitude can be seen. This result is consistent with the literature since longer distances between scatterers lead to smaller mode interactions.⁴⁹

In Figure 5, we compare the results for the structure in Figure 2c with the ones for the same system but made of gold. The preferential absorption of CPL by a chiral molecule is described by the dissymmetry factor, g , defined as follows⁶⁰

$$g = \frac{A^+ - A^-}{\frac{1}{2}(A^+ + A^-)} \approx -\left(\frac{G''}{\alpha''}\right)\left(\frac{2C}{\omega U_e}\right) \quad (2)$$

with $U_e = (\epsilon_0/4)\langle \tilde{E} \rangle^2$ being the time-average electric energy density. G'' and α'' are the molecule's chirality and electric polarizability, that is, the chiral asymmetry (g) in the absorption of light by a molecule is proportional to both the chirality of matter and the chirality of the electromagnetic field. This equation can be rewritten as follows⁶⁰

$$\hat{g} = \frac{g}{g_{\text{CPL}}} = \frac{2c}{\omega \epsilon_0} \frac{C}{|\tilde{E}|} \quad (3)$$

from where it can be noted that g can be enhanced above g_{CPL} by increasing the local density of chirality C or decreasing the local field intensity. In Figures 5a–d, we present the scattering-to-absorption cross-sectional ratios, the CD spectrum, and the dissymmetry factor \hat{g} for LCP and RCP polarizations, respectively. The same results are presented in the case of the structure made of gold in Figure 5e–h. We clearly observe large scattering-to-absorption ratios for the dielectric system, indicating a reduction in the losses' contribution when compared with their plasmonic counterparts. Moreover, a

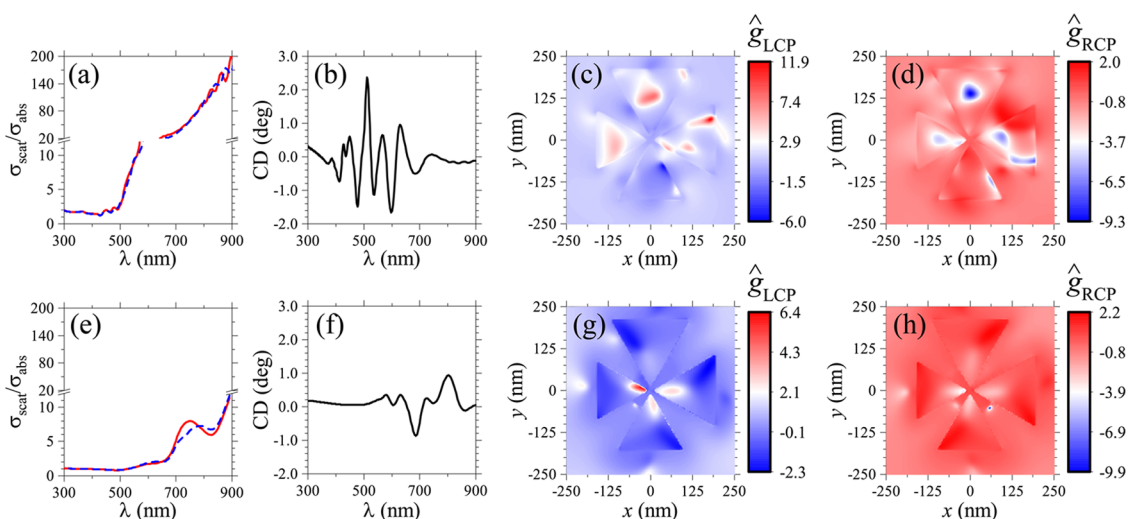


Figure 5. Ratio of the scattering to absorption, CD spectrum, and dissymmetry factors for LCP and RCP incident lights are presented for the systems made of (a–d) Si and (e–h) Au, respectively.

larger CD signal is also noted for the dielectric system. In Figures 5c,d and Figures 5g,h, we present the results for the dissymmetry factor, for both systems, for each polarization of the incident light. Results indicate that these systems exhibit a high chiroptical activity, large CD, and C fields with chiral hotspots. However, the main disadvantage of using chiral platforms, dielectric or plasmonic, is associated with the strong chiroptical background from the structure, as noted from the latter results. In this respect, symmetric structures from Figure 1, where C values are enhanced for each polarization, can be competitive with some recent proposals^{59–61} to improve CD measurements from dielectric nanoparticle systems.

The final objective of this work is to propose an all-dielectric chiral metasurface, as illustrated in the insets of Figure 6a,b, for

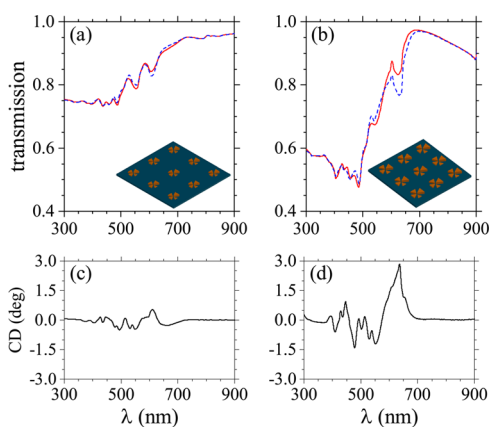


Figure 6. Transmission spectra for all-dielectric chiral metasurfaces, considered as built by the periodic repetition of the system studied in Figure 2f, with period lengths of (a) 800 nm and (b) 600 nm. Results are presented for RCP (solid) and LCP (dashed) incident lights. The corresponding CD spectra are presented in (c) and (d).

potential applications in highly efficient chiral biosensors. For this purpose and based on its high chiral optical activity, we considered the crossed-bowtie structure shown in Figure 2c as the unit cell to build the metasurface. It was arranged in a squared lattice with a size period length Δ concentric with the

central gap. The corresponding CD signal was calculated from the transmittance spectra as follows

$$\text{CD} = \tan^{-1} \left(\frac{T_{\text{RCP}} - T_{\text{LCP}}}{T_{\text{RCP}} + T_{\text{LCP}}} \right) \quad (4)$$

with T_{RCP} and T_{LCP} being the transmittances for RCP and LCP incident lights, respectively. The transmittance and CD spectra are shown in Figures 6a,b and Figures 6c,d, respectively, for $\Lambda = 800$ and 600 nm. The increase in chiral optical activity, while decreasing the length of the period, is explained by the increase in the overlap of the electric near-field tails between the neighboring cells. This can be noted from Figure 7, where we present the corresponding chiral near-fields, normalized by the C_{CPL} of the free-space-propagating CPL light, within a unit cell for periods $\Lambda = 800$ nm in Figure 7a,b and $\Lambda = 600$ nm in Figure 7c,d. Results are presented for RCP and LCP incident lights. It has been previously observed and explained^{55,56} that in the case of plasmonic nanoparticles, the near-field overlap

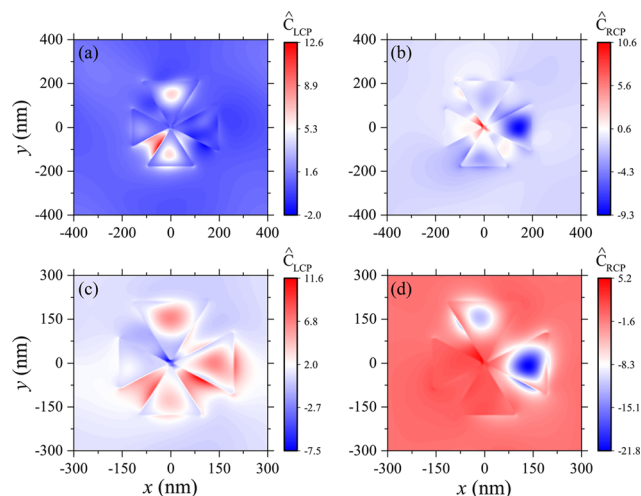


Figure 7. Normalized optical chirality near-fields for (a, b) $\Lambda = 800$ nm and (c, d) $\Lambda = 600$ nm. Results are presented for a unit cell. Results for nine unit cells can be seen in Figure S3 in the Supporting Information.

among neighboring scatterers resemble the electronic bands comprising well-localized atomic orbitals. Thus, we show here how to design the corresponding chiral “meta-atoms”, made as a crossed-bowtie systems, to build all-dielectric chiral metasurfaces with enhanced chiroptical responses. We also emphasize that the low-loss structure, observed from the scattering/absorption ratio for the unit cells, proposed in this work exhibits a CD spectral response higher than those in recent proposals that use complex plasmonic or hybrid nanostructures.^{52,57}

CONCLUSIONS

We have demonstrated that all-dielectric metasurfaces, consisting of a two-dimensional periodic arrangement of conveniently designed Si crossed-bowtie nanoantennas, can generate chiral hotspots and robust CD signals. Based on the separation distance of the crossed-bowtie systems, we can control the overlap between the corresponding electric and magnetic modes responsible for maximizing the optical chirality of the proposed metasurfaces. The corresponding electric hotspots are located at the central gap region, which opens up the possibility of using this metasurface for circular dichroism spectroscopy. Finally, it is worth mentioning that the proposed metasurface can be relevant in chiral biosensing applications, such as optical enantiomer discrimination after proper functionalization of the metasurface.⁵⁸ However, for a detection up to the single-molecule level, an array of symmetric systems can be better suited to avoid the strong background of CD from chiral bowties.

ASSOCIATED CONTENT

Supporting Information

The Supporting Information is available free of charge at <https://pubs.acs.org/doi/10.1021/acsomega.9b02381>.

Plots of the optical chiral near-fields for the structures in Figures 1, 3 and 7; results are normalized to the values of C associated with the circularly polarized incident light (CPL) at free-space (PDF)

AUTHOR INFORMATION

Corresponding Authors

*E-mail: pablo.albella@uicn.br (P.A.).

*E-mail: jrmeija@inatel.br (J.R.M.-S.).

ORCID

Pablo Albella: 0000-0001-7531-7828

Notes

The authors declare no competing financial interest.

ACKNOWLEDGMENTS

J.R.M.-S. acknowledges the financial support from the National Council for Scientific and Technological Development—CNPq (305958/2018-6, 429496/2018-4). F.R.G. thanks the financial support from the Colombian agency COLCIENCIAS. P.A. acknowledges funding from the Ramon y Cajal Fellowship RYC-2016-20831 and from Programa Viera y Clavijo de la Agencia Canaria de Investigación, Innovación y Sociedad de la Información (ACIISI). This work was also partially supported by RNP, with resources from MCTIC, Grant No. 01250.075413/2018-04, under the Radiocommunication Reference Center (Centro de Referência em Radiocomunicações—CRR) project of the National Institute of Tele-

communications (Instituto Nacional de Telecomunicações—Inatel), Brazil.

REFERENCES

- (1) Mogilner, A.; Fogelson, B. Cytoskeletal Chirality: Swirling Cells Tell Left from Right. *Curr. Biol.* **2015**, *25*, R501.
- (2) Hall, J. P.; Keane, P. M.; Beer, H.; Buchner, K.; Winter, G.; Sorensen, T. L.; Cardin, D. J.; Brazier, J. A.; Cardin, C. J. Delta Chirality Ruthenium ‘Light-Switch’ Complexes can Bind in the Minor Groove of DNA with Five Different Binding Modes. *Nucleic Acids Res.* **2016**, *44*, 9472.
- (3) Nguyen, L. A.; He, H.; Pham-Huy, C. Chiral Drugs: an Overview. *Int. J. Biomed. Sci.* **2006**, *2*, 85–100.
- (4) Tokunaga, E.; Yamamoto, T.; Ito, E.; Shibata, N. Understanding the Thalidomide Chirality in Biological Processes by the Self-Disproportionation of Enantiomers. *Sci. Rep.* **2018**, *8*, No. 17131.
- (5) Kelvin, W. T. B. *The Molecular Tactics of a Crystal*; Clarendon Press: Oxford, 1894.
- (6) Kelvin, W. T. B. *Baltimore Lectures on Molecular Dynamics and the Wave Theory of Light*; CJ Clay and Sons: Cambridge UK, 1904.
- (7) Rodger, A.; Nordén, B. *Circular Dichroism and Linear Dichroism*; Oxford University Press, 1997; Vol. I.
- (8) Bogdanov, A. A.; Shalin, A. S.; Ginzburg, P. Optical Forces in Nanorod Metamaterial. *Sci. Rep.* **2015**, *5*, No. 15846.
- (9) Wu, P. C.; Liao, C. Y.; Savinov, V.; Chung, T. L.; Chen, W. T.; Huang, Y.-W.; Wu, P. R.; Chen, Y.-H.; Liu, A.-Q.; Zheludev, N. I.; Tsai, D. P. Optical Anapole Metamaterial. *ACS Nano* **2018**, *12*, 1920–1927.
- (10) Engheta, N. Circuits with Light at Nanoscale: Optical Nanocircuits Inspired by Metamaterials. *Science* **2007**, *317*, 1698.
- (11) Cohen, M.; Shavit, R.; Zalevsky, Z. Enabling High Efficiency Nanoplasmonics with Novel Nanoantenna Architecture. *Sci. Rep.* **2015**, *5*, No. 17562.
- (12) Davis, T. J.; Gómez, D. E.; Roberts, A. Plasmonic Circuits for Manipulating Optical Information. *Nanophotonics* **2017**, *6*, 543–559.
- (13) Li, B.-B.; Clements, W. R.; Yu, X.-C.; Shi, K.; Gong, Q.; Xiao, Y.-F. Single Nanoparticle Detection Using Split-Mode Microcavity Raman Lasers. *Proc. Natl. Acad. Sci. U.S.A.* **2014**, *111*, 14657–14662.
- (14) Jeong, H.-H.; Mark, A. G.; Alarcón-Correa, M.; Kim, I.; Oswald, P.; Lee, T.-C.; Fischer, P. Dispersion and Shape Engineered Plasmonic Nanosensors. *Nat. Commun.* **2016**, *7*, No. 11331.
- (15) Kim, E.; Baaske, M. D.; Schuldes, I.; Wilsch, P. S.; Vollmer, F. Label-Free Optical Detection of Single Enzyme-Reactant Reactions and Associated Conformational Changes. *Sci. Adv.* **2017**, *3*, No. e1603044.
- (16) Wang, S. B.; Chan, C. T. Lateral Optical Force on Chiral Particles Near a Surface. *Nat. Commun.* **2014**, *5*, No. 3307.
- (17) Hayat, A.; Mueller, J. P. B.; Capasso, F. Lateral Chirality-Sorting Optical Forces. *Proc. Natl. Acad. Sci. U.S.A.* **2015**, *112*, 13190–13194.
- (18) Zhao, Y.; Saleh, A. A. E.; Dionne, J. A. Enantioselective Optical Trapping of Chiral Nanoparticles with Plasmonic Tweezers. *ACS Photonics* **2016**, *3*, 304–309.
- (19) Yue, Z.; Ren, H.; Wei, S.; Lin, J.; Gu, M. Angular-Momentum Nanometrology in an Ultrathin Plasmonic Topological Insulator Film. *Nat. Commun.* **2018**, *9*, No. 4413.
- (20) Fu, Y.; Hu, X.; Lu, C.; Yue, S.; Yang, H.; Gong, Q. All-Optical Logic Gates Based on Nanoscale Plasmonic Slot Waveguides. *Nano Lett.* **2012**, *12*, 5784–5790.
- (21) Cohen, M.; Zalevsky, Z.; Shavit, R. Towards Integrated Nanoplasmonic Logic Circuitry. *Nanoscale* **2013**, *5*, 5442–5449.
- (22) Brongersma, M. L.; Shalaev, V. M. The Case for Plasmonics. *Science* **2010**, *328*, 440–441.
- (23) Nesterov, M. L.; Yin, X.; Schäferling, M.; Giessen, H.; Weiss, T. The Role of Plasmon-Generated Near Fields for Enhanced Circular Dichroism Spectroscopy. *ACS Photonics* **2016**, *3*, 578–583.
- (24) Jack, C.; Karimullah, A. S.; Leyman, R.; Tullius, R.; Rotello, V. M.; Cooke, G.; Gadegaard, N.; Barron, L. D.; Kadodwala, M.

Biomacromolecular Stereostructure Mediates Mode Hybridization in Chiral Plasmonic Nanostructures. *Nano Lett.* **2016**, *16*, 5806–5814.

(25) Hentschel, M.; Schäferling, M.; Duan, X.; Giessen, H.; Liu, N. Chiral Plasmonics. *Sci. Adv.* **2017**, *3*, No. e1602735.

(26) Wang, X.; Tang, Z. Circular Dichroism Studies on Plasmonic Nanostructures. *Small* **2017**, *13*, No. 1601115.

(27) Kramer, C.; Schäferling, M.; Weiss, T.; Giessen, H.; Brixner, T. Analytic Optimization of Near-Field Optical Chirality Enhancement. *ACS Photonics* **2017**, *4*, 396–406.

(28) Tullius, R.; Platt, G. W.; Khorashad, L. K.; Gadegaard, N.; Laphorn, A. J.; Rotello, V. M.; Cooke, G.; Barron, L. D.; Govorov, A. O.; Karimullah, A. S.; Kadodwala, M. Superchiral Plasmonic Phase Sensitivity for Fingerprint of Protein Interface Structure. *ACS Nano* **2017**, *11*, 12049–12056.

(29) Zhao, Y.; Askarpour, A. N.; Sun, L.; Shi, J.; Li, X.; Alù, A. Chirality Detection of Enantiomers Using Twisted Optical Metamaterials. *Nat. Commun.* **2017**, *8*, No. 14180.

(30) Kong, X.-T.; Besteiro, L. V.; Wang, Z.; Govorov, A. O. Plasmonic Chirality and Circular Dichroism in Bioassembled and Nonbiological Systems: Theoretical Background and Recent Progress. *Adv. Mater.* **2018**, No. 1801790.

(31) Saito, K.; Tatsuma, T. Chiral Plasmonic Nanostructures Fabricated by Circularly Polarized Light. *Nano Lett.* **2018**, *18*, 3209–3212.

(32) Kelly, C.; Khorashad, L. K.; Gadegaard, N.; Barron, L. D.; Govorov, A. O.; Karimullah, A. S.; Kadodwala, M. Controlling Metamaterial Transparency with Superchiral Fields. *ACS Photonics* **2018**, *5*, 535–543.

(33) Wang, S.; Kang, L.; Werner, D. H. Active Terahertz Chiral Metamaterials Based on Phase Transition of Vanadium Dioxide (VO₂). *Sci. Rep.* **2018**, *8*, No. 189.

(34) Chen, Y.; Gao, J.; Yang, X. Chiral Metamaterials of Plasmonic Slanted Nanoapertures with Symmetry Breaking. *Nano Lett.* **2018**, *18*, 520–527.

(35) Reddy, I. V. A. K.; Baev, A.; Furlani, E. P.; Prasad, P. N.; Haus, J. W. Interaction of Structured Light with a Chiral Plasmonic Metasurface: Giant Enhancement of Chiro-Optic Response. *ACS Photonics* **2018**, *5*, 734–740.

(36) Kuznetsov, A. I.; Miroshnichenko, A. E.; Brongersma, M. L.; Kivshar, Y. S.; Luk'yanchuk, B. Optically Resonant Dielectric Nanostructures. *Science* **2016**, *354*, No. aag2472.

(37) Barreda, A. I.; Saiz, J. M.; Gonzalez, F.; Moreno, F.; Albella, P. Recent Advances in High Refractive Index Dielectric Nanoantennas: Basics and Applications. *AIP Adv.* **2019**, *9*, No. 040701.

(38) Evlyukhin, A. B.; Reinhardt, C.; Seidel, A.; Lukayanchuk, B. S.; Chichkov, B. N. Optical Resonance Features of Si-Nanoparticle Arrays. *Phys. Rev. B* **2010**, *82*, No. 045404.

(39) Gómez-Medina, R.; Garcia-Camara, B.; Saenz, J. J.; Suarez-Lacalle, I.; Gonzalez, F.; Moreno, F.; Nieto-Vesperinas, M. Electric and Magnetic Dipolar Response of Germanium Nanospheres: Interference Effects, Scattering Anisotropy, and Optical Forces. *J. Nanophotonics* **2011**, *5*, No. 053512.

(40) García-Etxarri, A.; Gomez-Medina, R.; Froufe-Perez, L. S.; Lopez, C.; Chantada, L.; Scheffold, F.; Aizpurua, J.; Nieto-Vesperinas, M.; Sáenz, J. J. Strong Magnetic Response of Submicron Silicon Particles in the Infrared. *Opt. Express* **2011**, *19*, 4815–4826.

(41) Liu, W.; Miroshnichenko, A. E. Scattering Invisibility with Free-Space Field Enhancement of All-Dielectric Nanoparticles. *Laser Photonics Rev.* **2017**, *11*, No. 1700103.

(42) Grinblat, G.; Li, Y.; Nielsen, M.; Oulton, R. F.; Maier, S. A. Enhanced Third Harmonic Generation in Single Germanium Nanodisks Excited at the Anapole Mode. *Nano Lett.* **2016**, *16*, 4635–4640.

(43) Shibamura, T.; Grinblat, G.; Albella, P.; Maier, S. A. Efficient Third Harmonic Generation from Metal-Dielectric Hybrid Nanoantennas. *Nano Lett.* **2017**, *17*, 2647–2651.

(44) Gongora, J. S. T.; Miroshnichenko, A. E.; Kivshar, Y. S.; Fratolocchi, A. Anapole Nanolaser for Mode-Locking and Ultrafast Pulse Generation. *Nat. Commun.* **2017**, *8*, No. 15535.

(45) Geffrin, J. M.; Garcia-Camara, B.; Gómez-Medina, R.; Albella, P.; Froufe-Pérez, L. S.; Eyraud, C.; Litman, A.; Vaillon, R.; Gonzalez, F.; Nieto-Vesperinas, M.; Saenz, J. J.; Moreno, F. Magnetic and Electric Coherence in Forward and Backscattered Electromagnetic Waves by a Single Dielectric Subwavelength Sphere. *Nat. Commun.* **2012**, *3*, No. 1171.

(46) Staude, I.; Miroshnichenko, A. E.; Decker, M.; Fofang, N. T.; Liu, S.; Gonzales, E.; Dominguez, J.; Luk, T. S.; Neshev, D. N.; Brener, I.; Kivshar, Y. Tailoring Directional Scattering Through Magnetic and Electric Resonances in Subwavelength Silicon Nanodisks. *ACS Nano* **2013**, *7*, 7824.

(47) Shibamura, T.; Maier, S. A.; Albella, P. Polarization Control of High Transmission/Reflection Switching by All-Dielectric Metasurfaces. *Appl. Phys. Lett.* **2018**, *112*, No. 063103.

(48) Barreda, A. I.; Saleh, H.; Litman, A.; Gonzalez, F.; Geffrin, J.; Moreno, F. Electromagnetic Polarization-Controlled Perfect Switching Effect with High Refractive-Index Dimers and the Beam-Splitter Configuration. *Nat. Commun.* **2017**, *8*, No. 13910.

(49) Albella, P.; Poyli, M. A.; Schmidt, M. K.; Maier, S. A.; Moreno, F.; Saenz, J. J.; Aizpurua, J. Low-Loss Electric and Magnetic Field-Enhanced Spectroscopy with Subwavelength Silicon Dimers. *J. Phys. Chem. C* **2013**, *117*, 13573.

(50) Caldarola, M.; Albella, P.; Cortes, E.; Rahmani, M.; Roschuk, T.; Grinblat, G.; Oulton, R. F.; Bragas, A. V.; Maier, S. A. Non-Plasmonic Nanoantennas for Surface Enhanced Spectroscopies with Ultra-Low Heat Conversion. *Nat. Commun.* **2015**, *6*, No. 7915.

(51) Ullah, K.; Garcia-Camara, B.; Habib, M.; Liu, X.; Krasnok, A.; Lepeshov, S.; Hao, J.; Liu, J.; Yadav, N. P. Chiral All-Dielectric Trimer Nanoantenna. *J. Quant. Spectrosc. Radiat. Transfer* **2018**, *208*, 71–77.

(52) Mark, A. G.; Gibbs, J. G.; Lee, T.-C.; Fischer, P. Hybrid Nanocolloids with Programmed Three-Dimensional Shape and Material Composition. *Nat. Mater.* **2013**, *12*, 802.

(53) Palik, E. D. *Handbook of Optical Constants of Solids*; Elsevier Inc., 1985.

(54) Schäferling, M.; Yin, X.; Giessen, H. Formation of Chiral Fields in a Symmetric Environment. *Opt. Express* **2012**, *20*, 26326.

(55) Ito, T.; Sakoda, K. Photonic Bands of Metallic Systems. II. Features of Surface Plasmon Polaritons. *Phys. Rev. B* **2001**, *64*, No. 045117.

(56) Halas, N. J.; Lal, S.; Chang, W.-S.; Link, S.; Nordlander, P. Plasmon in Strongly Coupled Metallic Nanostructures. *Chem. Rev.* **2011**, *111*, 3913–3961.

(57) George, J.; Kar, S.; Anupriya, E. S.; Somasundaran, S. M.; Das, A. D.; Sissa, C.; Painelli, A.; Thomas, K. G. Chiral Plasmons: Au Nanoparticle Assemblies on Thermoresponsive Organic Templates. *ACS Nano* **2019**, *13*, 4392–4401.

(58) Kinkhabwala, A.; Yu, Z.; Fan, S.; Avlasevich, Y.; Müllen, K.; Moerner, W. E. Large Single-Molecule Fluorescence Enhancements Produced by a Bowtie Nanoantenna. *Nat. Photonics* **2009**, *3*, 654–657.

(59) Yoo, S. J.; Park, Q. H. Enhancement of Chiroptical Signals by Circular Differential Mie Scattering of Nanoparticles. *Sci. Rep.* **2015**, *5*, No. 14463.

(60) Ho, C.-S.; Garcia-Etxarri, A.; Zhao, Y.; Dionne, J. Enhancing Enantioselective Absorption Using Dielectric Nanospheres. *ACS Photonics* **2017**, *4*, 197–203.

(61) Vestler, D.; Ben-Moshe, A.; Markovich, G. Enhancement of Circular Dichroism of a Chiral Material by Dielectric Nanospheres. *J. Phys. Chem. C* **2019**, *123*, 5017–5022.